Title

Nanocrystal Dynamics: Spontaneous Reshaping and Splitting of AgCl Nanocrystals under Electron Beam Illumination (Small 48/2018)

Journal

Small, 14(48)

ISSN

1613-6810

Authors

Tian, Xuezeng
Anand, Utkarsh
Mirsaidov, Utkur
et al.

Publication Date

2018-11-01

DOI

10.1002/smll.201870231

WILEY-VCH

DOI: 10.1002/ ((please add manuscript number))

Article type: Full Paper

Spontaneous reshaping and splitting of AgCl nanocrystals under electron beam illumination

*Xuezeng Tian[1,2], Utkarsh Anand[3,4,5], Utkur Mirsaidov[3,4,5], Haimei Zheng[2,6]**

Dr. X. Tian, Prof. H. Zheng

Materials Sciences Division, Lawrence Berkeley National Laboratory, Berkeley, CA 94720

Department of Materials Science and Engineering, University of California, Berkeley, CA 94720

Berkeley Education Alliance for Research in Singapore, 138602, Singapore

E-mail: hmzheng@lbl.gov

U. Anand, Prof. U. Mirsaidov

Center for BioImaging Sciences, Department of Biological Sciences, National University of Singapore, 117557, Singapore

Department of Physics, National University of Singapore, 117551, Singapore

Centre for Advanced 2D Materials and Graphene Research Centre, National University of Singapore, 117546, Singapore

Keywords: AgCl nanomotors, charged nanocrystals, shape instability, liquid cell, *in situ* transmission electron microscope

Abstract: AgCl is photosensitive thus often used as micromotors. However, the dynamics of individual AgCl nanoparticle motion in liquids upon illumination remains elusive. Here, using liquid cell transmission electron microscope (TEM) we observe AgCl nanocrystals reshaping and splitting spontaneously in an aqueous solution under electron beam illumination. We find the AgCl nanocrystals are negatively charged in the liquid environment, where the charge induces a repulsive Coulomb force that reshapes and stretches those nanocrystals. Upon extensive stretching, the AgCl nanocrystal splits into small nanocrystals and each nanocrystal retracts back into cuboid shapes due to cohesive surface. Our analysis shows that each nanocrystal maintains a single crystal rocksalt structure during splitting. The splitting of AgCl nanocrystals is analogous to the electrified liquid droplets or other reported Coulomb fission phenomena, but with distinctive structural properties. Revealing of the dynamic behavior of AgCl nanocrystals opens the opportunity to explore their potential applications as actuators for nanodevices.

1. Introduction

AgCl is photosensitive, thus micrometer sized AgCl particles have frequently been reported as photoactivated micromotors which convert photon energy into mechanical energy to produce motion.[1-4] For instance, upon ultra-violet (UV) light illumination, AgCl particles immersed in water decompose into Ag and chloric acid (HCl). The produced protons diffuse much faster than chloride ions (D_{H^+} = 9.311×10^{-5} cm^{2}s^{-1}, D_{Cl^-} = 1.385×10^{-5} cm^{2}s^{-1}), resulting in an electrolyte gradient which generates an electric field.[5, 6] The electrolyte gradient leads to ionic diffusiophoresis which provides a driving force for the nanoparticles to move. Asymmetric photodecomposition may cause directional particle motion.[7, 8] The reduced Ag metal can be plated onto the particles as the AgCl are consumed in the above experiments, which slows down the nanoparticle motion. It has also been reported that when H_2O_2 is added

to the AgCl-UV light system, the reduction of AgCl to Ag by UV light and the oxidation of Ag to AgCl by peroxide produce and consume HCl. This competition and the associated gradient reversal lead to periodic attraction and repulsion between colloids, thus oscillatory motion of the particles.[9] The facile chemical conversion of AgCl particles and the associated dynamic motion are fascinating. However, little is known about structural instability and motion of AgCl nanoparticles in liquids due to the lack of direct observation with high spatial resolution.

Here, we report the spontaneous reshaping and splitting of AgCl nanocrystals in an aqueous solution induced by electron beam illumination, which are achieved using *in situ* liquid cell transmission electron microscopy (TEM). A nanofabricated liquid cell from ultra-thin silicon wafers is composed of two liquid reservoirs and an electron transparent SiN_x membrane window (each membrane is 20 nm-thick). We load the precursor solution of 10-100 mM KCl aqueous solution with Ag nanoparticles into one of the reservoirs and the solution is drawn into the cell by capillary force forming a thin liquid layer sandwiched between the SiN_x membranes[10-13] (see Experimental Section). AgCl nanocrystals are formed under electron beam irradiation. All AgCl nanocrystals are more or less faceted nanocuboids with rectangles or deformed rectangles in the two-dimensional projection (see Supporting Information (SI)-Section 1 and 2). AgCl nanocrystals become unstable under electron beam illumination. When the electron dose rate is above a certain threshold, they undergo drastic reshaping and splitting events. More than a hundred splitting events are observed, of which we record movies at the rate of 10 frames per second. The electron beam dose rate is maintained at 0-40 $e/(Å^2 \cdot s)$ as specified in each case.

2. Spontaneous reshaping and splitting of AgCl nanocrystals

The schematic in **Figure 1**a shows a typical splitting event of a AgCl nanocrystal revealed through liquid cell TEM. There are three stages during the splitting event: lateral stretching of

the AgCl nanocrystal preferred at the corner(s), splitting of the primary nanocrystal, and retracting of the secondary AgCl nanocrystals into nanocuboids. Figure 1b and 1c show two typical splitting events stretching out from the corners of AgCl nanocrystals, which are abrupt and explosive. More examples of explosive splitting are available in SI-Section 5. It is noted that all of those explosive splitting events are initiated at the nanocrystal corners. The projected size of the AgCl nanocrystal increases up to three times of the original size during the stretching, as shown by the size evolution plotted in Figure 1e and 1f. Subsequently, splitting of the AgCl nanocrystal is observed. After splitting, all secondary nanocrystals retract into rectangular shapes. From the observation, we hypothesize that two counterbalanced forces are regulating the reshaping and splitting process, i.e., a repulsive force that stretches the nanocrystals and a cohesive force that retracts the AgCl nanocrystals. We will discuss the origin of this drive force further in detail in a later section of this paper.

Another type of splitting without the explosive characteristics is also observed, which is associated with much larger AgCl nanocrystals. Figure 1d shows a large AgCl nanocrystal (~ 385 nm) expands from the interior by first forming holes, then holes become larger and the nanocrystal eventually splits into many pieces. The holes are accounted to the weak points induced by radiolysis. After splitting, each piece transforms from the irregular shape into a nanocubiod and is stabilized. Comparing with the typical explosive processes, those mild splitting events exhibit three stages: premature stretching, splitting from edge or interior weak region, and retraction. The overall effect is the same with explosive splitting: to re-allocate the charges (decreasing the Coulomb energy), and increase the total surface area (increasing surface energy). Finally the system is stabilized, but through a different splitting approach.

3. AgCl nanocrystals are single crystalline and change shape like liquids

The facile processes of AgCl nanocrystal reshaping, splitting and retracting highlight the fluidity or of AgCl nanocrystals. Considering that AgCl nanocrystal reshaping and merging

are an intraparticle atomic diffusion process, we can estimate the viscosity of the AgCl nanocrystals with a simplified model using Stokes equation. Taking the merging of two nanocrystals in Figure 2a as an example, the merging process is regarded as a self-diffusion process with a finite velocity (~50 nm/s), where Stokes dragging force is counter-balanced by surface tension. With measured nanocrystal size, merging velocity and estimated surface tension (0.35 J/m^2),[14] the viscosity of the merging nanocrystal is estimated to be 2.3×10^6 Pa · s (see SI-Section 6 for details). Similarly, Figure 2b shows a large nanocrystal splits and the secondary pieces retract with a finite retraction velocity, which can be used to estimate the dynamic viscosity. The viscosity of 3.9×10^5 Pa · s is achieved in this case. Therefore, the viscosity of AgCl in this experiment is in the order of 10^5~10^6 Pa·s, which is within the range of molten glass.[15] AgCl is known to be radiation sensitive and has been used as the photographic film. Under electron beam irradiation, ionic bonding between Ag^+ and Cl^- ions are broken due to radiolysis resulting in silver reduction.[16] The observed liquid-like behaviors of the AgCl nanocrystals arises from the massive bond breaking due to electron beam induced radiolysis.

We have taken selected area electron diffraction (SAED) patterns during the nanocrystal reshaping and splitting processes. **Figure 3** shows a nanocrystal (P) splits into three (P, Q and R) pieces and the corresponding electron diffraction patterns at different stages. The original AgCl nanocrystal (P) is single crystalline along [001] zone axis (time 32.0 s). After splitting, three independent diffraction patterns corresponding to each individual AgCl nanocrystals (P, Q, and R) are achieved (time 35.5 s). Each nanocrystal is single-crystalline with face-centered cubic (FCC) rocksalt structure and the primary (100) terminating facets. This has been confirmed by additional measurements of a large number of nanocrystals (see **Figure S2** in SI), which is consistent with the crystal habit of AgCl nanocrystals.[16] The orientation of diffraction patterns matches the shape of each AgCl nanocrystal very well, as shown in Figure

3b and 3c. When the nanocrystal P rotates 10° clockwise (from time 35.5 s to 39.8 s), the corresponding diffraction of P also rotates by the same angle; while as the nanocrystal Q and R remain stationary, their diffraction patterns also remain stationary.

4. Rayleigh instability and Coulomb fission

We further find that AgCl nanocrystals reshaping is highly dependent on the electron dose rate. In **Figure 4**a, the morphology of five nanocrystals with various sizes can be manipulated between near the spherical nanoparticles and the faceted cuboids by changing the electron dose rate. Under low electron dose rate (1 e/(Å^2·s)), surface tension dominates thus the nanocrystals with rounded corners are observed. Higher electron dose rate (5 e/(Å^2·s) or higher) induces nanocrystals with more well-defined corners. **Figure 4**b shows the shape evolution of a AgCl nanocrystal highlighting the electron dose effects. Under high electron dose rate (13 e/(Å^2·s)), the nanocrystal is highly stretched with an irregular shape (time 0.1 s to 5.9 s). When the electron dose rate decreases to 1 e/(Å^2·s), the nanocrystal quickly retracts into a single rounded nanoparticle (time 6.0 s to 6.4 s). This suggests that the repulsive force counter-balancing the surface tension is largely removed with a lower electron dose rate.

Figure 4c shows statistics of the nanocrystal sizes in various splitting events under different electron dose rate. Large nanocrystals (e.g., edge length over 200 nm) may split under significantly lower electron dose rate (~3 e/(Å^2·s)). Smaller nanocrystals require a higher dose rate to split. Various of splitting events are observed under the electron dose of 0-35 e/(Å^2·s). Nanocrystals smaller than 30 nm do not split under even much higher electron dose rate (>40 e/(Å^2·s)). It is also noted that electron beam induced reduction of AgCl into Ag clusters are found when the electron dose rate is above 40 e/(Å^2·s) (see SI Section 10). However, when the electron dose rate is below 40 e/(Å^2·s), no obvious decomposition of AgCl nanocrystals is observed. It is also noted that many AgCl nanoparticles move in the same direction within the

field of view, which is likely due to the fluid flow or an electric field gradient from inhomogeneous electron beam density.

Electron beam is known to influence a sample in multiple ways, including heating, charging, induced radiation pressure and photochemical reactions (see SI-Section 8, 9, 10).[17,18] We consider the electron beam induced radiolysis and the accompanied charging effects are responsible for the observed reshaping and splitting of the AgCl nanocrystals. The AgCl nanocrystal surface in KCl solution can be highly negatively charged due to Cl^- adsorption, which is modulated by radiolysis related redox reactions.[16] Thus, a repulsive electrostatic force can be generated which stretches the AgCl nanocrystal. Simultaneously, the surface tension retracts the nanocrystal. The interplay between these two factors induces the rich dynamics of AgCl nanocrystal stretching, splitting and retracting.

Under the electron beam irradiation, AgCl immersed in water is known to decompose into Ag and HCl.[4-6, 9] However, in our experiments, a Ag oxidation process must be accompanied by the Ag^+ reduction since no obvious Ag plating was observed. It's well-established that radiolysis of water under the electron beam generates hydrated electrons, protons and oxidative hydrogen peroxides, which could induce redox reactions of AgCl:

$$4AgCl + 4H_2O \overset{e-beam}{\longleftrightarrow} 4Ag + 4H^+ + 4Cl^- + 2H_2O_2 \quad (1)$$

The reverse reaction of Ag oxidation into AgCl consumes the H^+ near the nanocrystals. Given the fact that the produced H^+ diffuses much faster than Cl^- in the forward reaction, a Cl^- rich inside/H^+ rich outside ionic gradient is formed. A dynamic equilibrium preventing the AgCl nanocrystals from decomposition into Ag metals can be established. The estimated ion distribution around the AgCl nanocrystal under the dynamic equilibrium is illustrated in **Figure 5a**. The surface of AgCl nanocrystals is known to be easily adsorbed with Cl^- due to

strong Ag^+-Cl^- affinity on the first Helmholtz layer, and be further screened by outer layer ions (e.g., H^+).[19-21]

The reshaping and splitting dynamics of AgCl nanocrystals fits well with Rayleigh's instability theory on Coulomb fission. Coulomb fission was first reported on electrified droplets,[22-25] which become unstable with a critical charge Q_c (known as Rayleigh limit) when the repulsive Coulomb force is equal to the cohesive surface tension. Recent high-speed optical microscopy studies have revealed the detailed Coulomb fission dynamics of a liquid droplet.[26-28] Coulomb fission has also been applied to a variety of charged solids, spanning from femtometer structures of nuclei (e.g., radium-228)[29, 30] to nanometer structures of large molecules (e.g., proteins),[31, 32] metal clusters (e.g., gold or sodium clusters),[33-35] and carbon-based materials (e.g., fullerene or nanotubes).[36-38] A similar Coulomb fission model can be applied to the observed electron beam induced splitting of AgCl nanocrystals. When the adsorbed charges reach the Rayleigh limit, explosive Coulomb fission results in drastic ejection of the charges and splitting of the nanocrystal into smaller pieces. After splitting, charges on the original nanocrystal are distributed on the smaller pieces. Thus, the overall electrostatic energy decreases due to the charge redistribution, whereas the surface energy increases due to increased surface area. Surface tension dominates the smaller pieces and it retracts the irregular shaped particles into nanocuboids. The larger nanocrystals exhibiting the mild splitting events, such as the cases in **Figure 1**d, may be induced by non-uniform surface charges and/or surface tension and defects inside the nanocrystal may have played a role.

In order to quantify the scale of electrostatic repulsion, we use the Finite Element Method (FEM) to simulate the electric field distribution of a AgCl nanocrystal in KCl solution. We assume an evenly distributed surface charge density allowing the average electrostatic force equals the surface tension. Our simulation shows that the edges and corners of the nanocrystal experience the maximum electric field (**Figure 5b**). This explains why stretching originates

from the corners of a nanocrystal. When the repulsive force is larger than the surface tension, the AgCl nanocrystal becomes unstable and the spontaneous reshaping and stretching of AgCl nanocrystals can be achieved.

We further analyze the morphological transition of AgCl from a round nanoparticle into a more faceted nanocuboid from the viewpoint of Gibbs free energy (such as the case in Figure 3a). The Gibbs free energy change of the system ΔG can be expressed by:

$$\Delta G = \Delta E_C + \Delta E_\sigma + \Delta E_V = \Delta\, Q^2/2C_s + \sigma\Delta A + \Delta E_V \quad (2)$$

where, E_C is the Coulomb energy, E_σ is the interfacial free energy, E_V is the bulk free energy of the AgCl crystal, Q is the charge amount on a nanocrystal, σ is the surface tension. C_s and R_s are the capacitance and equivalent radius of the ball-like AgCl nanocrystals (see SI-Section 2). During splitting, ΔE_C is negative and ΔE_σ is positive. ΔE_V is positive because any reshaping in solid materials should overcome an energy barrier. But due to the electron beam induced radiolysis, the AgCl NCs exhibit liquid-like behaviors where the strong ionic bonds are already massively broken. Here, we approximate the critical charge by assuming ΔE_V is zero. For example, for a nanocrystal with radius of 50 nm, the minimum charge is 10980e, which equals to a charge density of 0.31 e/nm^2. Whereas the critical charge for a nanocrystal with radius of 25 nm is 3882e, which equals to a charge density of 0.44 e/nm^2. The smaller nanocrystals require a higher charge density to reshape and split.

5. Conclusion

In summary, we have observed spontaneous reshaping and splitting of single crystalline AgCl nanocrystals using liquid cell TEM. The results show that AgCl nanocrystals maintain the single crystal lattice during the splitting event. The reshaping and splitting of AgCl arise from the interplay between the repulsive electrostatic force and the cohesive surface tension. The directional splitting of AgCl nanocrystals initiated at the corners is distinctly different from the splitting of electrified droplets or other reported Coulomb fission, while high flexibility of

the AgCl nanocrystal is observed. This work opens the opportunity to further study Coulomb fission of solids and explore potential applications as actuators in nanodevices.

6. Experimental Section

Liquid cells and instruments. An *in situ* fluid stage (Hummingbird Scientific, USA) was used in this experiment. No spacer is applied on the SiNx windows, but due to the surface is not perfectly clean, a liquid layer of 100-200 nm was usually obtained. All the *in situ* experiments were carried out using a JEOL 2010F microscope operating at 200 keV. A bubble in the middle of the SiN_x window was formed to introduce a thin liquid region.

Preparation of AgCl nanocrystals. The AgCl was formed by immersing silver nanocrystals in potassium chloride (KCl) solution. The silver nanocrystals were formed by depositing 1nm silver onto the SiN_x membrane of SiN_x chip using thermal evaporator.[39] Then KCl solution was loaded into the liquid cell. Under electron irradiation, chloride ions facilitate the oxidative dissolution of silver and AgCl precipitates near the SiN_x membrane.[40] The concentration of the KCl solution we used was 10mM, 25mM, 40mM, and 100mM. All four concentrations ensure a chloride-excess environment. No obvious difference was observed.

Electric Field Simulation. We have applied Poisson equation based on the simulation software COMSOL™ to simulate the electric field distribution. The surface charge density was set to be Rayleigh limit, which is 0.052 C/m^2, or 0.327 e/nm^2. The static dielectric constant of AgCl at room temperature is 11.14. The static dielectric constant of 10 mM KCl at room temperature is 78. More details are in SI-Section 4.

Supporting Information

Supporting Information is available from the Wiley Online Library or from the author.

Acknowledgements

This work was funded by U.S. Department of Energy, Office of Science, Office of Basic Energy Sciences, Materials Sciences and Engineering Division under Contract No. DE-AC02-05-CH11231 within the insitu TEM program (KC22ZH). X.Z. acknowledges the support of SinBeRise program of Berkeley Education Alliance for Research in Singapore (BEARS). U.M. acknowledges the supports from the Singapore Ministry of Education under Academic Research Fund Tier 2 (MOE2016-T2-2-009). X.T. thanks Jingyu Lu, Zainul Aabdin and Qi Liu for their help with the guidance on experimental set up.

Received: ((will be filled in by the editorial staff))

Revised: ((will be filled in by the editorial staff))

Published online: ((will be filled in by the editorial staff))

References

[1] P. Illien, R. Golestanian, A. Sen. *Chem. Soc. Rev.* **2017,** 46, 5508-5518..

[2] M. Safdar, J. Simmchen, J. Janis. *Enviro. Sci.: Nano* **2017,** 4, 1602-1616.

[3] L. Xu, F. Mou, H. Gong, M. Luo, J. Guan. *Chem. Soc. Rev.* **2017,** 46, 6905-6926.

[4] A. Sen, M. Ibele, Y. Hong, D. Velegol. *Faraday Discuss.* **2009,** *143*, 15-27.

[5] I. Michael, M. T. E., S. Ayusman. *Angew. Chem., Int. Ed.* **2009,** 48, 3308-3312.

[6] W. Duan, M. Ibele, R. Liu, A. Sen. *Eur. Phys. J. E* **2012,** 35, 77.

[7] J. L. Anderson. *Annu. Rev. Fluid Mech.* **1989,** 21, 61-99.

[8] C. Zhou, H. P. Zhang, J. Tang, W. Wang. *Langmuir* **2018,** *34*, 3289-3295.

[9] M. E. Ibele, P. E. Lammert, V. H. Crespi, A. Sen. *ACS Nano* **2010,** *4*, 4845-4851.

[10] H. Zheng, R. K. Smith, Y.-w. Jun, C. Kisielowski, U. Dahmen, A. P. Alivisatos. *Science* **2009,** *324*, 1309-1312.

[11] U. M. Mirsaidov, H. Zheng, D. Bhattacharya, Y. Casana, P. Matsudaira. *Proc. Natl. Acad. Sci. U. S. A.* **2012,** 109, 7187-7190.

[12] H.-G. Liao, D. Zherebetskyy, H. Xin, C. Czarnik, P. Ercius, H. Elmlund, M. Pan, L.-W. Wang, H. Zheng. *Science* **2014,** *345*, 916-919.

[13] Z. Zeng, W.-I. Liang, H.-G. Liao, H. L. Xin, Y.-H. Chu, H. Zheng. *Nano Lett.* **2014,** *14*, 1745-1750.

[14] Z. Lou, B. Huang, X. Ma, X. Zhang, X. Qin, Z. Wang, Y. Dai, Y. Liu. *Chem. Eur. J.* **2012,** 18, 16090-16096.

[15] H. R. Lillie. *J. Rheol* **1932,** 3, 121-126.

[16] Tani, T., *Photographic Science: Advances in Nanoparticles, J-Aggregates, Dye Sensitization, and Organic Devices*. OUP Oxford: 2011.

[17] D. B. Williams, C. B. Carter, *Transmission Electron Microscopy: A Textbook for Materials Science*. Springer: 2009.

[18] L. Reimer, H. Kohl, *Transmission Electron Microscopy: Physics of Image Formation*. Springer New York: 2008.

[19] K. R. Temsamani, K. Lu Cheng. *Sensor. Actuat. B-Chem.* **2001,** 76, 551-555.

[20] K. L. Cheng. *Microchem. J.* **2002,** *72*, 269-276.

[21] H. Tamagawa, S. Morita. *Membranes* **2014,** *4*, 257-274.

[22] L. Rayleigh. *Phil. Mag. S.5.* **1882,** 14, 184-186.

[23] C. D. Hendricks. *J. Colloid Sci.* **1962,** 17, 249-259.

[24] A. Doyle, D. R. Moffett, B. Vonnegut. *J. Colloid Sci.* **1964,** 19, 136-143.

[25] D. C. Taflin, T. L. Ward, E. J. Davis. *Langmuir* **1989,** *5*, 376-384.

[26] K. Tang, A. Gomez. *Phys. Fluids* **1994,** 6, 2317-2332.

[27] T. Achtzehn, R. Müller, D. Duft, T. Leisner. *Eur. Phys. J. D* **2005,** 34, 311-313

[28] D. Duft, T. Achtzehn, R. Muller, B. A. Huber, T. Leisner. *Nature* **2003,** *421*, 128-128.

[29] S. Frankel, N. Metropolis. *Phys. Rev.* **1947,** *72*, 914-925.

[30] P. Moller, D. G. Madland, A. J. Sierk, A. Iwamoto. *Nature* **2001,** *409*, 785-790.

[31] J. Jortner, I. Last, Y. Levy. *Int. J. Mass spectrom.* **2006,** *249–250*, 184-190.

[32] M. Vonderach, O. T. Ehrler, K. Matheis, T. Karpuschkin, E. Papalazarou, C. Brunet, R. Antoine, P. Weis, O. Hampe, M. M. Kappes, P. Dugourd. *Phys. Chem. Chem. Phys.* **2011,** 13, 15554-15558.

[33] F. Chandezon, S. Tomita, D. Cormier, P. Grubling, C. Guet, H. Lebius, A. Pesnelle, B. A. Huber. *Phys. Rev. Lett.* **2001,** *87*, 153402.

[34] F. Calvo. *Phys. Rev. A* **2006,** *74*, 043202.

[35] M. Bär, B. Faber, P. G. Reinhard, P. M. Dinh, E. Suraud, P. Wopperer. *J. Phys. Conf. Ser.* **2010,** 248, 012023.

[36] G. Liu, Y. Zhao, K. Zheng, Z. Liu, W. Ma, Y. Ren, S. Xie, L. Sun. *Nano Lett.* **2009,** *9*, 239-44.

[37] A. J. Stace, E. Bichoutskaia. *Phys. Chem. Chem. Phys.* **2011,** 13, 18339-18346.

[38] X. Wei, D.-M. Tang, Q. Chen, Y. Bando, D. Golberg. *ACS Nano* **2013,** *7*, 3491-3497.

[39] C. Binns. *Surf. Sci. Rep.* **2001,** *44*, 1-49.

[40] K. Loza, J. Diendorf, C. Sengstock, L. Ruiz-Gonzalez, J. M. Gonzalez-Calbet, M. Vallet-Regi, M. Koller, M. Epple. *J. Mater. Chem. B* **2014,** 2, 1634-1643.

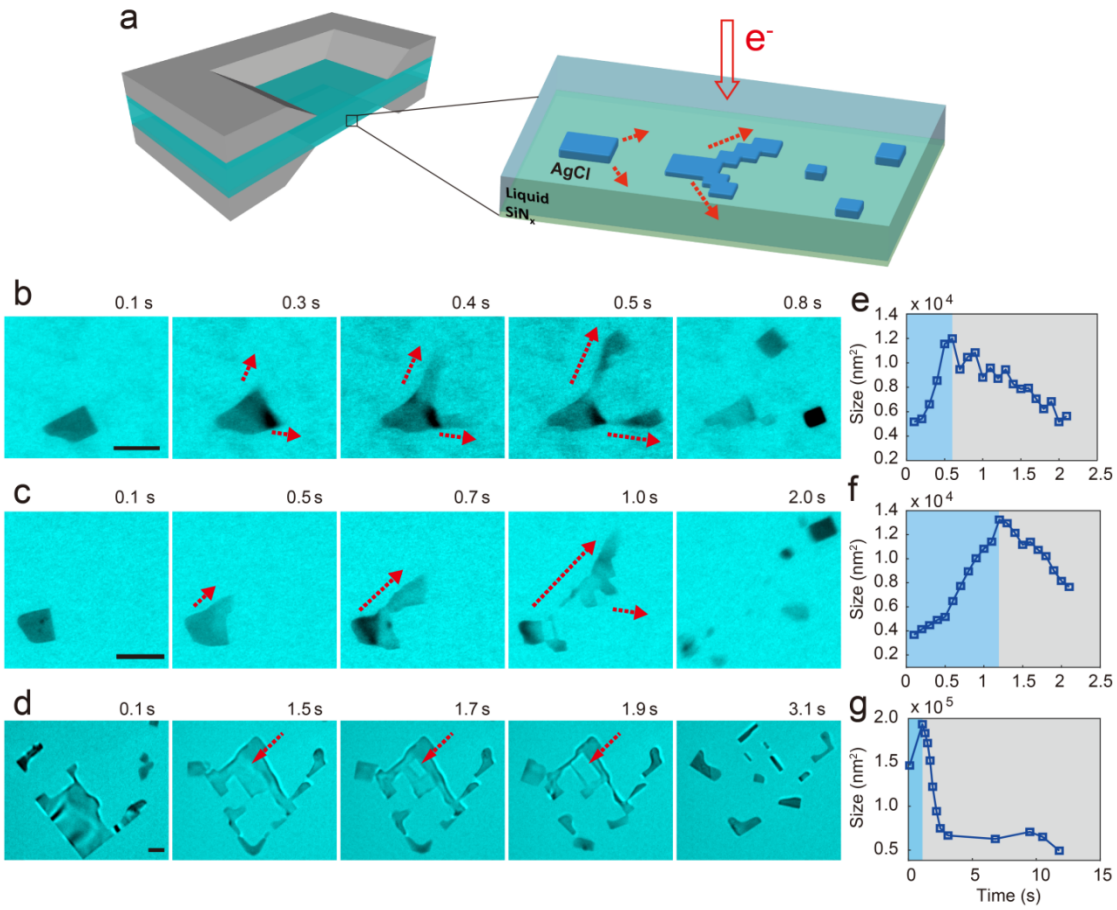

Figure 1. Typical spontaneous reshaping and splitting of AgCl nanocrystals in liquid cell under electron beam illumination. (a) Schematic representation of stretching, splitting, and retraction of AgCl nanocrystal during a splitting event. (b) Sequential TEM images showing the explosive splitting starting from two corners of a AgCl nanocrystal. The red arrows show the nanocrystal stretching directions during the splitting process. (c) Sequential TEM images showing the explosive splitting from one corner of a AgCl nanocrystal. (d) A gradual splitting event initiated from the interior of a AgCl nanocrystal. The red arrow indicates the initial splitting points. (e-g) The projected size evolution with time for the corresponding nanocrystals shown in (b-d). All scale bars are 100 nm. Electron dose rate was maintained at 13 e/(Å^2·s) for the above cases.

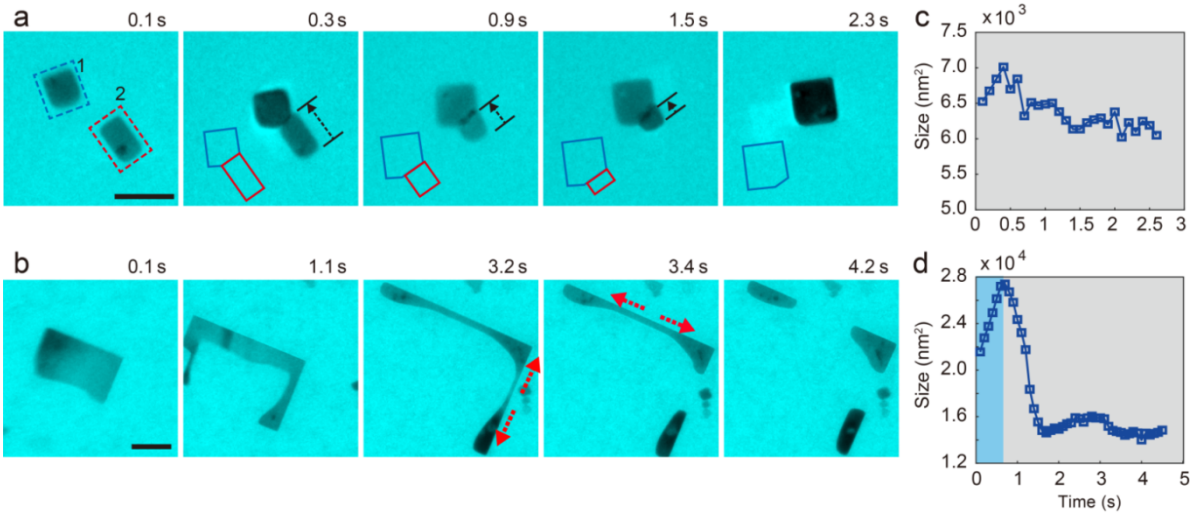

Figure 2. Merging and stretching of AgCl nanocrystals show the liquid-like behavior of nanocrystals. (a) Two AgCl nanocrystals merging together with a finite merging velocity of 50 nm/s. Using Stokes equation, the dynamic viscosity here is estimated to be 2.3×10^6 Pa · s. (b) A large nanocrystal stretching and splitting into pieces with a finite splitting velocity. The maximum retracting speed is about 300nm/s. The dynamic viscosity here is estimated to be 3.9×10^5 Pa · s. (c-d) Size evolution corresponding to the dynamic processes in (a) and (b), respectively. The scale bars are 100 nm.

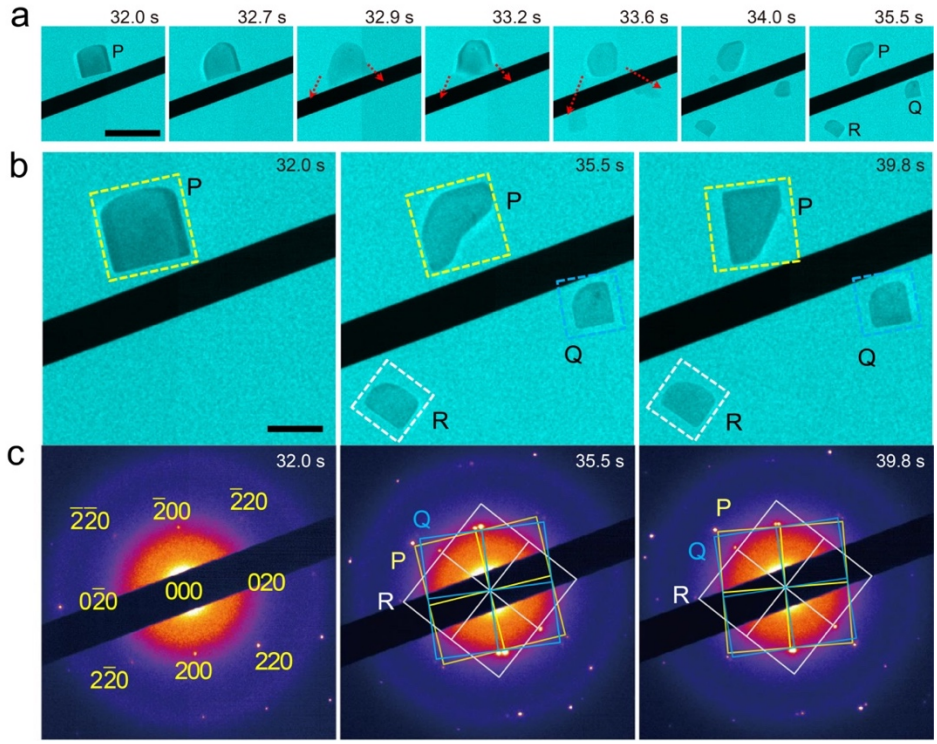

Figure 3. AgCl nanocrystals maintain single crystalline structure during splitting. (a) Sequential TEM images showing a typical splitting event initiated from two corners of the nanocrystal. Arrows indicate splitting directions. The black bar in the middle is the beam stopper. During the splitting process, the electron dose rate is manipulated between 4-13 e/(Å^2·s). Scale bar is 500 nm. (b) TEM images showing different states of splitting event, where the nanocrystal "P" splits into "P", "Q" and "R". Edges of the surrounding boxes are parallel to the nanocrystal straight edges. The colors of the boxes are consistent with the electron diffraction patterns in (c). Scale bar is 200 nm. (c) Each electron diffraction pattern corresponding to the contributing nanocrystals in (b): P, Q, and R. The Bragg spots are all indexed to be AgCl with the lattice constant of 5.55 Å and along [001] zone axis.

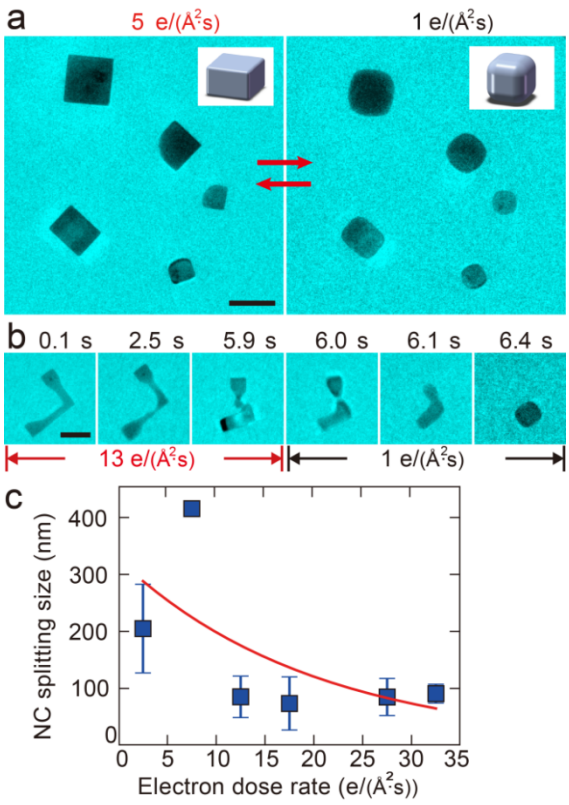

Figure 4. The electron dose rate dependent AgCl reshaping and splitting. (a) Reversible morphological changes dependent on the electron beam dose rate. (b) AgCl nanocrystal stretches and splits under high electron beam dose rate (13 e/(Å^2·s)) and it retracts into a rod

nanoparticle under low electron beam dose rate (1 e/(Å^2·s)). All scale bars are 100 nm. (c) Statistics of nanocrystal (NC) sizes in various splitting events under different electron dose rate.

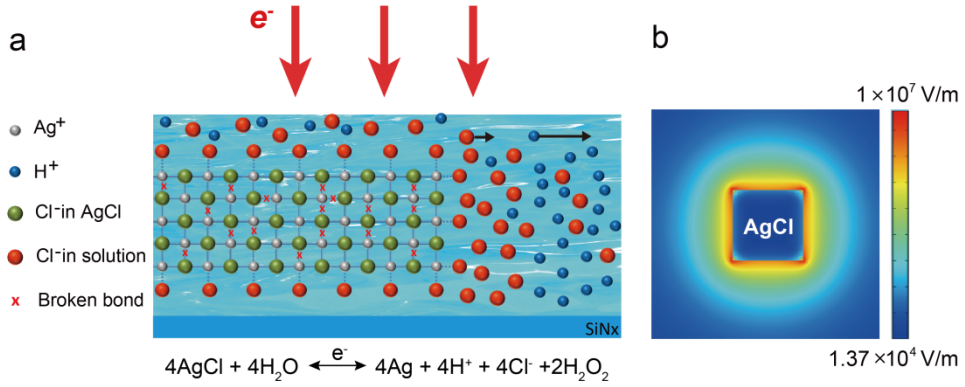

Figure 5. Mechanisms of Coulomb fission of AgCl nanoparticles in an aqueous solution under electron beam illumination. (a) Schematic of AgCl redox reaction in KCl solution under an electron beam. The reaction equation combines the AgCl decomposition due to electron beam illumination and recovery due to oxidants (H_2O_2) generated by the interaction of electron beam with water. The arrows on Cl^- and H^+ show the difference in diffusion speed resulting in an electrolyte gradient. (b) Finite Element Method (FEM) simulation of electric field distribution assuming an evenly distributed surface charge with a charge density of 0.327 e/nm^2.

Nanomotors based on individual AgCl nanocrystals demonstrate rich dynamics of spontaneous reshaping and splitting as imaged by liquid cell transmission electron microscopy. All AgCl nanocrystals maintain single crystalline while simultaneously exhibits liquid-like behaviors. Charging related Rayleigh instability accounts for regulating the dynamics. This work improves understanding of AgCl based nanomotors and inspires new designing and applications.

Keyword: AgCl nanomotors, charged nanocrystals, shape instability, liquid cell, *in situ* transmission electron microscope

*Xuezeng Tian, Utkarsh Anand, Utkur Mirsaidov, Haimei Zheng**

Spontaneous reshaping and splitting of AgCl nanocrystals under electron beam illumination

ToC figure:

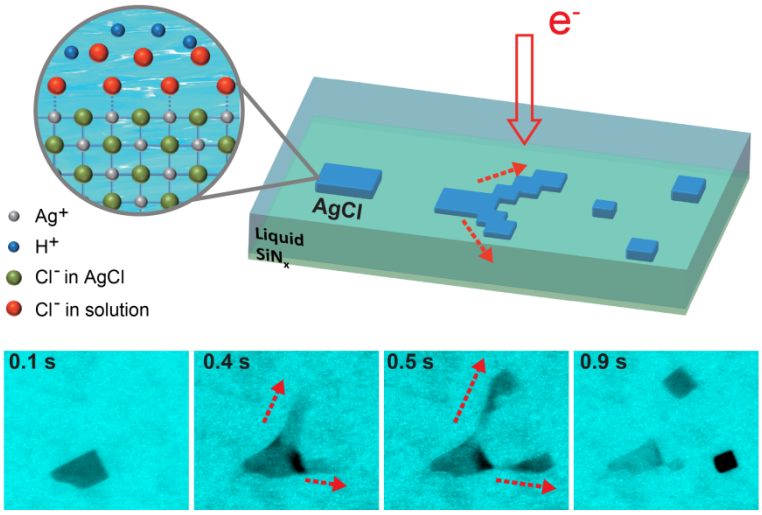

Supporting Information

Spontaneous reshaping and splitting of AgCl nanocrystals under electron beam illumination

*Xuezeng Tian, Utkarsh Anand, Utkur Mirsaidov, Haimei Zheng**

Table of contents

1. Shape evolution and energetics of AgCl nanocrystals.

Figure S1 shows the newly formed AgCl nanocrystals.[1, 2] Agglomerations of small AgCl nanocrystals into large ones are frequently observed. In this work, we focus on the shape changes of individual AgCl nanocrystals. The AgCl nanocrystals are sensitive to electron beam and liquid environment. When totally immersed in the solution, as Figure S1A, they could reshape but couldn't split. When they are on dried region without solution surrounded, they reshape and decompose, but do not split. Only when they are confined in a thin liquid layer (bubble region of liquid cell) and exposed to electron dose rate that they spontaneously reshape and split. In the manuscript, all the dynamics was captured in the thin liquid layer.

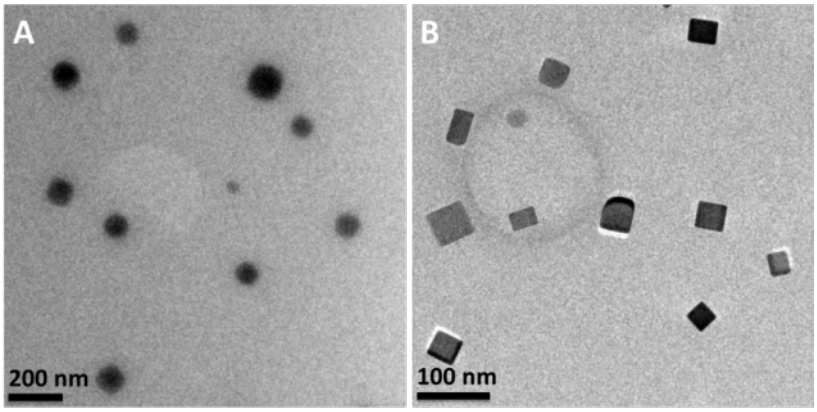

Figure S1. Preparation of AgCl nanocrystals in a liquid cell. (a) Newly formed AgCl nanoparticles. (b) The AgCl nanoparticles become more faceted transforming into thin plates (bubble region).

We model the AgCl nanoparticles as a "superball" structure. In mathematics, a superball structure can be expressed by an extension of the equation for a sphere:

$$|x|^{2s} + |y|^{2s} + |z|^{2s} = |a|^{2s}, \quad \text{(S1)}$$

where s is the shape parameter and a is the equivalent radius for the superballs.[1] s can vary between 1 and infinity corresponding to a sphere and a cube, respectively. As to the superballs in the experiment shown in Figure 4a in main text, we find s is approximately 1.5 for

nanocrystals under low dose, and 10 for nanocrystals under high dose.

Figure S2. Superball structures whose surface by definition corresponds to $|x|^{2s} + |y|^{2s} + |z|^{2s} = a^{2s}$. From left to right the *s* values are 1, 1.5, 2.5, 10 and ∞. Thus, the spheres and cubes are unified with the same definition.

It's also noted that, in the calculation of Gibbs free energy in main text, E_σ is the interfacial energy between AgCl surface and KCl aqueous solution, which is approximately 0.35 J/m^2, or 0.35 N/m.[3] Self-capacitance *C* and hydrodynamic radius *R* can be further determined using the above stated superball structure according to Audus, *et al.*[2] When $s_1 = 1.5$, we get $C_{s1} \sim 1.006C_0$, $R_{s1} \sim 1.006R_0$; when $s_2 = 10$, we get $C_s = 1.06C_0$, $R_s = 1.06R_0$. Here C_0 and R_0 are the self-capacitance and radius of sphere with same volume, and $C_0 = 4\pi\varepsilon\varepsilon_0 R_0$, where ε is the dielectric constant ($\varepsilon_{\mathrm{AgCl}} = 11.14$), ε_0 is the vacuum permittivity ($\varepsilon_0 \approx 8.854\times10^{-12}$ F m^{-1}).

In main manuscript Figure 4a, the superballs reshaped from $s_1 = 1.5$ to $s_2 = 10$. According to equation (2) and assuming ΔE_V is zero, we get:

$$Q^2/2C_{s2} + 4\pi\sigma R_{s2}^2 - Q^2/2C_{s1} - 4\pi\sigma R_{s1}^2 \leq 0, \quad \text{(S2)}$$

which gives:

$$Q \geq 4\pi R_0\sqrt{2\sigma R_0\varepsilon\varepsilon_0 \times sc_1 \times sc_2 \times (sc_1 + sc_2)}, \quad \text{(S3)}$$

Where sc_1 and sc_2 are the superball scale factor 1.006 and 1.06, respectively. Given the radius R_0, we can get the minimum charge Q to reshape a superball nanocrystal. For example,

when R_0=50nm, we get $Q \geq 10980e$; while R_0=25nm, we get $Q \geq 3882e$. We found the charge density for reshaping of AgCl nanocrystals is 0.29 e/nm^2 for R_0=50nm and 0.41 e/nm^2 for R_0=25nm, which is larger than the Rayleigh limit of equivalent droplets. The equation for Rayleigh limit charge of liquid droplets is shown below,[4] which is defined as the Coulomb energy reaches twice the surface energy:

$$Q = 8\pi R_0 \sqrt{\sigma R_0 \varepsilon \varepsilon_0}, \quad \text{(S4)}$$

But the nanocrystals are still stable under this charge density, showing only slightly shape transform. We believe the enhanced stability of nanocrystals over droplets is due to the bulk free energy E_V, which contains anisotropic ionic bonding in AgCl rather than isotropic intermolecular forces in liquids. The ionic bonding does not only make the nanocrystals more stable than droplets, but also limits the morphological transition trajectories. Thus, the morphological transition of AgCl nanocrystals upon charging follows the crystalline infrastructures. Rayleigh limit of AgCl nanocrystals should be larger than that for liquid droplets in order to overcome the ionic binding energy.

2. Morphology-Orientation Correspondence (MOC)

From the correspondence between diffractions and nanocrystal morphologies, we find all of the small AgCl nanocrystals are faceted by (100) planes with zone axis [001]. Based on this result, we make an assumption of Morphology-Orientation Correspondence (MOC) that we use a rectangle to envelope an AgCl nanocrystal, where the rectangle facets are (100) planes with zone axis [001]. **Figure S3** shows more examples of MOC. From numerous comparisons between diffractions and crystal morphologies, we all find this MOC relationship. If the nanocrystals reshape, at least two neighboring facets remain rectangular shape, from which we can still judge the orientation. As AgCl has a stable cubic rocksalt structure, it's reasonable to have such MOC relationship from the viewpoint of crystallography.[5] It's not possible to

capture the electron diffraction for every individual nanocrystal during observation. Such a MOC relationship greatly facilitates our data analysis.

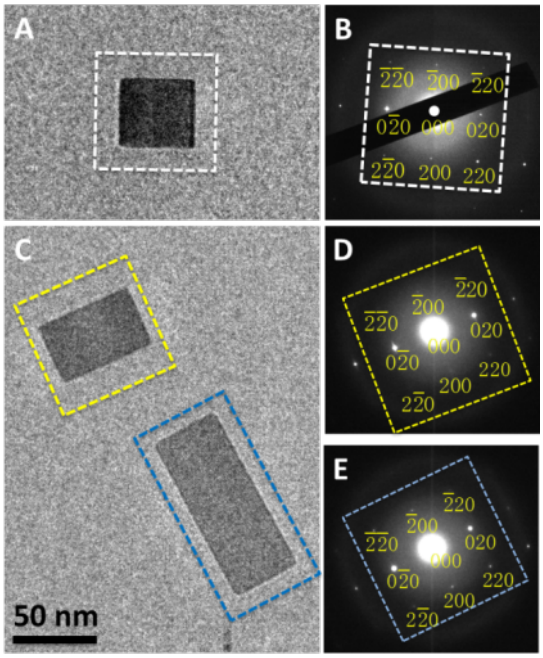

Figure S3. Examples of MOC. The corresponding nanocrystals and diffractions are labeled with the same colored rectangles. Nearest and second nearest diffraction spots are indexed.

3. Thickness estimate

We have estimated the thickness of the AgCl nanocrystals by comparing the relative intensity of the transmitted electrons through the AgCl nanocrystals (N_{AgCl}) and through the non-nanocrystal region (N_0):

$$N_{AgCl}/N_0 = \exp(-t/\lambda), \quad \text{(S5)}$$

where t is the thickness of AgCl nanocrystal, and λ is the mean free path of AgCl (λ = 81.8 nm). Thus, by measuring N_{AgCl} and N_0 we get the thickness. This is a rough estimate since diffraction contrast of AgCl may have significant impact. In order to minimize the diffraction contrast of AgCl in the thickness estimation, we choose AgCl nanocrystals off zone axis. For the example shown in **Figure S4**, the thickness is estimated to be about 29.4 nm. We find the

nanocrystal thickness before splitting (as those shown in the movies) ranges from a few nanometers to 60 nm.

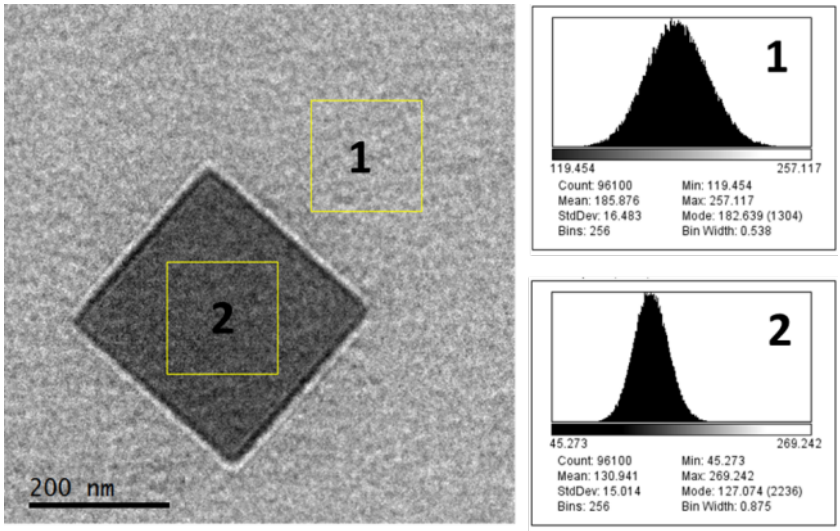

Figure S4. An example of thickness estimation. Region 2 shows a nanocrystal with average count 131, while region 1 is nanocrystal free with average count 186. The thickness of this nanocrystal is thus estimated to be 29.4 nm.

4. Finite Element Method (FEM) simulation

We have applied Poisson equation based on the simulation software COMSOL™ to simulate the electric field distribution:

$$\Delta u = -\rho/\varepsilon\varepsilon_0, \tag{S6}$$

where u is the electric potential, and ρ is the charge density. Take the nanocrystal in Figure 1b as a model nanocrystal. Using equation S3 we can get the Rayleigh limit charge as 7381e. The Rayleigh limit charge density is 0.052 C/m^2, or 0.327 e/nm^2. During the FEM simulation, we assume a Rayleigh limit charge amountis uniformly distributed on the surface of the AgCl nanocrystals. The static dielectric constant of AgCl at room temperature is 11.14.[5] The static dielectric constant of 10 mM KCl at room temperature is 78.[6] Dirichlet boundary condition was used where voltage at infinity is zero.

The simulation was performed to a 3D nanocrystal with length of 80 nm. In order to display the results, we have used slicing method to show the electric field distribution on a specific plane (Figure 6 in main text and **Figure S5**). It is noted that electric field distributions on different slicing planes are highly different. The image in Figure 6 is the slicing with plane z = 0 nm (taking the origin of coordinates to be the center of the nanocrystal), which shows electric field distribution of the cross-section through the nanocrystal (scales from 1.3×10^4 to 8.75×10^7 V/m). While Figure S5 shows the slicing with plane z = 40 nm, which is the electric field distribution on the nanocrystal top surface (scales from 5.58×10^6 to 9.54×10^7 V/m).

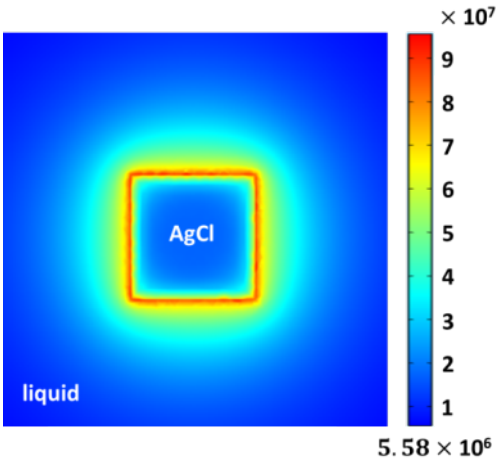

Figure S5. FEM simulation of electric field distribution of AgCl nanocrystal in 10 mM KCl (nanocrystal edge length is 80nm). This image shows the slicing of result with plane z = 40 nm (the middle plane profile). The minimum of electric field is labeled (unit in V/m).

5. More splitting events analysis

Three typical splitting events showing different splitting trajectories. **Figure S6**a shows the splitting is dominated by two neighboring branches shooting out independently. Figure S6b exhibits a splitting event without actually splitting into many small pieces, but only two pieces. Figure S6c shows one splitting event superseded by another splitting event continuously. The

continuous splitting result in the flat plot in **Figure S7**c. All splitting events show the three stages of Coulomb fission as stretching, splitting and retracting of the nanocrystal (Figure S7).

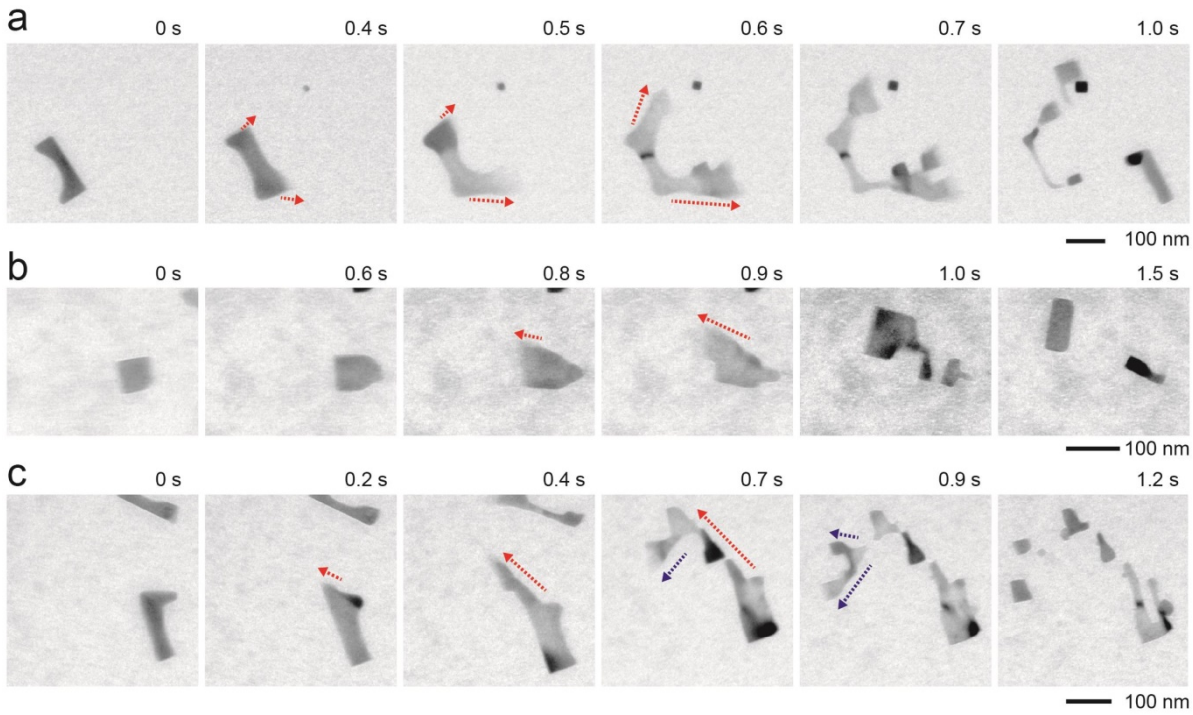

Figure S6. More splitting events. The time of each frame is labelled. The arrows in the images indicate the direction and length of the splitting branches. The blue arrows in (c) indicate the secondary splitting while red arrows the primary one.

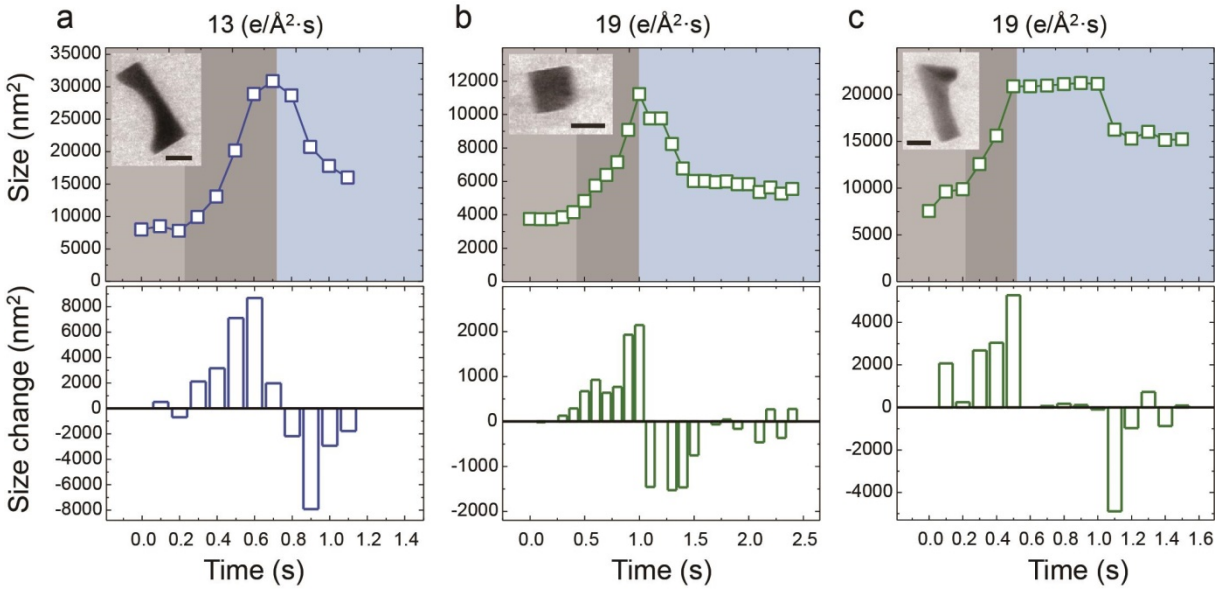

Figure S7. Analysis on splitting events of Figure S6. Top panels show the projected size evolution corresponding to Figure S6a, S6b and S6c, respectively. Bottom panels show the

size change rate at different stages. All splitting events show similar behavior of three stages Coulomb fission as described in main text.

6. Liquid-like behaviors of AgCl nanocrystal

The AgCl nanocrystals show softened features under electron beam irradiation. During the experiments, we have frequently observed spontaneous nanocrystal reshaping and coalescence. In the main text, **Figure 2**a shows the coalescence of two neighboring nanocrystals with a different orientation. After the two nanocrystals attach, one nanocrystal absorbs the other, and a larger single crystalline nanocrystal is achieved quickly in 2 seconds. Such coalescence behavior is different from our former experiments on gold nanoparticle coalescence, where two gold nanoparticles in attachment don't merge fully.[7] In the current study, AgCl nanocrystals merge fully with ease, indicating a low energy barrier to eliminating the interfaces between AgCl nanocrystals.

As we have discussed, the morphology and dynamics of nanocrystals rely on the balance between repulsive Coulomb force and cohesive surface tension. When two stable nanocrystals meet, cohesive surface tension is dominant thus they merge into one. We consider the surface tension exclusively as the driving force for nanocrystals to merge:

$$F_\sigma = \sigma \cdot 2\pi R_\sigma, \tag{S7}$$

where F_σ is the surface force, R_σ is the cross-section radius of the merging nanocrystal.

The merging process is regarded as a self-diffusion process, where Stokes dragging force is considered:

$$F_S = 6\pi\mu\upsilon R_H, \tag{S8}$$

where F_S is the dragging force, μ is the dynamic viscosity, υ is the self-diffusing speed. R_H is the hydrodynamic radius of the diffusing nanocrystal, which is comparable with R_σ.

Here, we simplify the model in the following way: for two contacted NCs, the surface tension tends to merge them together; meanwhile the Stokes dragging force causes a resistance to the merging. Thus, a specific merging velocity is resulted due to the balance of the two forces, as illustrated in **Figure S8**. Our assumption oversimplifies the Stokes equation model, but we believe our estimation is within the accuracy of order of magnitude.

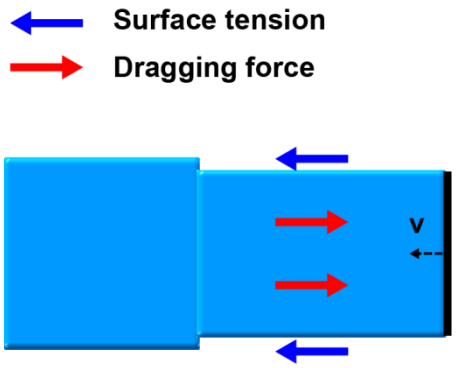

Figure S8. Schematic showing the balance between surface tension and the dragging force during two NCs merge. In order to use equation (S8), we measure the moving speed v of the end of merging NC (shown by black line). Similar to that of a standard viscosity measurement by moving a sphere in a viscous liquid, the black line is moving towards the larger NC by expelling the AgCl itself. The specific velocity of the black line is due to the balance between the dragging force and surface tension.

By balancing the surface force with Stokes dragging force, and given the surface tension $\sigma = 0.35\ \mathrm{N/m}$ and speed v we get the dynamic viscosity of AgCl. In Figure 2a, the nanocrystal on the right is consumed with a speed of 50 nm/s. The corresponding dynamic viscosity is about $2.3 \times 10^6\ \mathrm{Pa \cdot s}$.

A similar estimation can be applied to a reshaping nanocrystal, as shown in Figure 2b. When

the nanocrystal is thin enough (on the edge in Figure 2b), it breaks due to Plateau–Rayleigh instability.[8] After the splitting, surface tension contracts the elongated particle with a speed of v. The maximum contracting speed in Figure 2b is about 300nm/s. Thus, we get dynamic viscosity about 3.9×10^5 Pa · s. According to the above discussion, we conclude that the AgCl nanocrystals in KCl solution are fluidic with dynamics viscosity $10^5 \sim 10^6$ Pa · s.

7. Drifting motion and Coulomb fission induced motion of AgCl nanocrystals

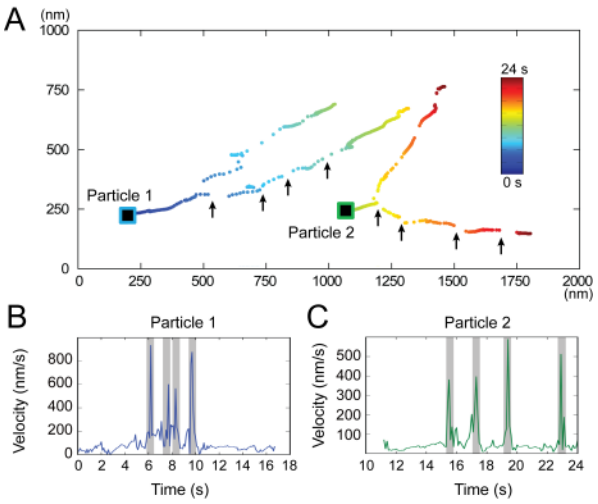

Figure S9. Influence of Coulomb fission on nanocrystal dynamics. (a) Trajectory of two splitting nanocrystals during Coulomb fission, as labelled on the image. The nanocrystals are drifting towards the observation window edge. The black arrows indicate the splitting events. (b-c) The nanocrystal velocity profiles of particle 1 and particle 2, respectively. The velocity profiles correspond to the trajectories highlighted with arrows. The shadowed regions show the Coulomb fission events, in correspondence with the arrows in (a).

We further study the dynamics of the splitting nanocrystals. The splitting events create new nanocrystals from the original nanocrystals with a fast speed. In **Figure S9**, we analyze the trajectories of two drifting nanocrystals highlighting the splitting events. Each nanocrystal split several times into many new nanocrystals while drifting following the flow of liquid near

the window edge. The splitting events can be observed as discontinuity in the trajectory indicated by arrows. The drift speed is about 60 nm/s, while the explosive splitting at the shooting-out point is as fast as 800 nm/s. All the peaks in velocity profiles correspond to the splitting events. The explosive splitting may alter the direction of nanocrystal movement. The trajectories of the nanocrystals always redirect during the splitting events, as indicated by the arrows. The splitting event always start from the neighboring two corners of a rectangular nanocrystal. The smaller nanocrystals ejected from the mother-nanocrystal follow their own drifting directions.

8. Heating effect due to direct energy transfer from electron beam

Here we evaluate how much the electron beam influence the temperature of the nanocrystal-liquid-SiN_x membrane system. We consider the system to be a two layer system where liquid layer is on SiN_x membrane and AgCl nanocrystals reside in the liquid layer, which can be further averaged as a 2D system. Ignoring the heat loss through other mechanisms (i.e., convective flow), the temperature increase of the 2D membrane can be calculated using a cylindrical heat conduction equation:

$$-k \cdot \left(\frac{d^2T}{dr^2} + \frac{1}{r}\frac{dT}{dr}\right) = J, \tag{S9}$$

where k is thermal conductivity, temperature T is a function of radius r, and J is heat flux density. The thermal conductivity k is 0.58 W/m·K for water, 1.8 W/m·K for SiN_x thin film, and 1.15 W/m·K for AgCl, at room temperature.[9] We take the average k as 0.5 W/m·K to see an overestimated maximum of temperature.

The heat flux density J can be estimated by assuming all the electron energy loss transfers into heat, thus J is the multiplication of electron dose rate (normally in e/Å^2·s) and electron

energy loss rate (normally in eV/nm). The electron dose rate was recorded simultaneously when recording the movies. The electron energy loss rate can be calculated using Bethe formula:[10]

$$-\frac{dE(s)}{ds} = 2\pi N_0 e^4 \rho \frac{Z}{A}\frac{1}{E(s)} ln\left(\frac{aE(s)}{I}\right), \quad \text{(S10)}$$

where E is the electron energy, s is the distance along the path, Z and A are the average atomic number and atomic weight of a material, N_0 is Avogadro's number, e is electronic charge, ρ is the density of the material, I is the mean excitation energy of a material and can be estimated by $I=(9.76+58.8/Z^{-1.19})\cdot Z$ (in eV) and a is a constant (a=1.1658 for relativistic electron energy). The calculated electron energy loss rate is 0.61 eV/nm for water, 0.75 eV/nm for SiN_x and 0.13 eV/nm for AgCl. We take the energy loss rate as 0.2 eV/nm to see an overestimated maximum of heat flux. We use 20 e/Å^2·s as the upper limit of electron dose rate. Transferring all the units into SI unit, we get the heat flux density J as 6.4×10^{10} W/m^3.

According to our experiments, the electron beam size D_1 is dependent on electron dose rate and is about 3 μm under normal experiment condition. While the window size of our liquid cells is normally 10μm, we assume a circular shape of the window with radius D_0= 10μm. The edge of D_0 is the silicon chip which can be viewed as the heat sink with constant temperature 300K. With all the parameters and boundary conditions set, we simulated the temperature distribution on 2D, as shown in **Figure S10**. The maximum temperature increase is 0.2K, which is negligible to the nanocrystals.

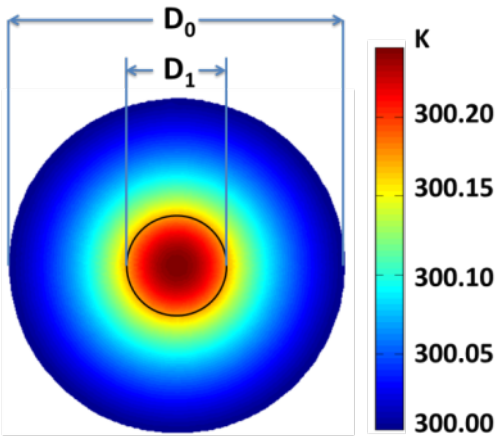

Figure S10. FEM simulation of temperature distribution due to electron beam heating. D_0 is the radius of the chip (D_0=10μm), and D_1 is the radius of electron beam radiation (D_1=3μm).

9. Radiation pressure due to direct momentum transfer from electron beam

The radiation pressure comes from the momentum transfer during bombardment of electrons on the materials. Thus only the scattered electrons need to be considered, which is given by:

$$N_{scatt}=N_{incid}-N_{out}=N_{incid}(1-\exp(-t/\lambda)), \quad \text{(S12)}$$

where N_{scatt} is the scattered electrons, N_{incid} is the incident electrons, N_{out} is the non-scattered electrons, t is the thickness of material and λ is the mean free path of electrons in the material.

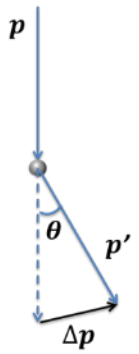

Figure S11. Schematic of momentum transfer due to electron bombardment.

For each scattered electron, the momentum change $\Delta p = 2psin\,\theta/2$, where θ is the scattering

angle and p is the incident electron momentum $\sqrt{2m_eE}$, where m_e is the mass of electron and E is the incident electron energy. The radiation pressure comes from the vertical component of the momentum change, which is $\Delta psin\,\theta/2 = 2psin^2\,\theta/2 = p(1-cos\theta)$. The scattering angle follows the Rutherford scattering rule. Here, for simplicity, we assume all the electrons are scattered back with $\theta = 180°$, that is, each scattered electron will have $2p$ momentum transfer on the vertical component. This momentum change exerts a force and therefore a pressure to the radiated material. Given $m_e = 9.1 \times 10^{-31}$ kg, E = 200 keV, incident electron dose rate = 20 e/Å^2·s, thickness of AgCl nanocrystal = 30 nm, electron mean free path in AgCl = 82 nm, we get the radiation pressure as 0.302 Pa, which is negligible comparing with atmospheric pressure in liquid cell (~10^5 Pa) or Laplace pressure inside the AgCl nanocrystal (~10^7 Pa).

10. Radiolysis of AgCl nanocrystals under electron beam

AgCl is known to be sensitive to radiations, either photons, electrons, or other high energy particles.[11] It should be noted that only under mild electron flux (1~30 e/Å^2·s) and thin liquid layer region could the spontaneous splitting happen. High electron dose rate leads to decomposition. We have observed electron induced decomposition of AgCl into Ag under two conditions: in the interior of large AgCl aggregates under high electron dose rate (>40 e/Å^2·s); or when the AgCl nanocrystals are located on dry region without liquid surrounding (~15 e/Å^2·s). But for AgCl nanocrystals immersed in Cl^- rich solution, they didn't decompose under the same dose rate. Thus, we propose the stabilization and adsorption effect of Cl^- ions, as discussed in main text.

Figure S12a shows the decomposition of a large AgCl nanocrystal, with dark Ag nanocrystals inside the bulk of it. It is noted that phase segregation of Ag and AgCl will happen. The

decomposition of AgCl results in Ag atoms dispersed in the framework of AgCl, while we frequently observed the Ag phase in small nanocrystal form, and small Ag phases tend to form larger phase. It's also noted an orientation correspondence exists between the segregated Ag phase and AgCl phase, as indicated by the diffraction (Figure S12b). An Ag (111) spot is always accompanied by an AgCl (111) spot, or Ag (200) spot accompanied by AgCl (200) spot, in exactly the same directions. This tells us the segregated Ag phase prefers the same orientation with the bulk AgCl phase. At electron dose rate as high as 80 e/Å^2·s, the AgCl nanocrystals subjected to severe decomposition problem.

Figure S12c and S12d show the decomposition of an AgCl nanocrystal on a relative dry area. A higher dose will instantly make the AgCl nanocrystal decompose into small dark Ag nanocrystals. For nanocrystals surrounded by KCl solution, we didn't find obvious decomposition. We attribute this stability to the excessive chloride ion in KCl solution, where a new chemical equilibrium may contribute. Whenever the AgCl is decomposed near the surface, it soon gets restored by the excessive KCl solution, therefore the AgCl nanocrystals appear stable.

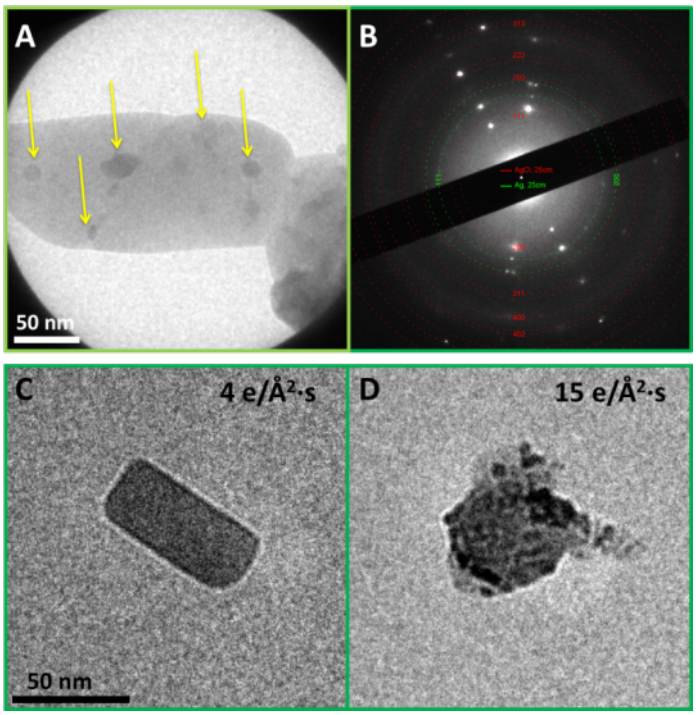

Figure S12. Electron beam induced AgCl decomposition. (a) Large AgCl particles with Ag phase inside. The arrows indicate the Ag phase inside the AgCl. (b) Diffraction pattern of (A). The diffraction rings are indexed to either AgCl (red) or Ag (green). (c) An AgCl nanocrystal on a dry area. (d) Decomposition of the nanocrystal in (c).

11. Movie captions

Movie S1. A typical splitting event of AgCl nanocrystal. The electron dose rate was kept at 13 e/(Å^2·s).

Movie S2. A single AgCl nanocrystal split into three smaller nanocrystals. The electron dose rate was kept at around 4 e/(Å^2·s) initially and increased to around 16 e/Å^2·s. The black bar is the beam stopping bar to protect screen.

Movie S3. Coalescence of two small AgCl nanocrystals. The electron dose rate was kept at 30 e/(Å^2·s).

Movie S4. A splitting event of AgCl nanocrystal. The electron dose rate was kept at 13 e/(Å^2·s).

Movie S5. Reshaping and splitting of a medium sized AgCl nanocrystal. The electron dose rate was kept at 13 e/(Å^2·s).

Movie S6. Reshaping and splitting of a large sized AgCl nanocrystal. The electron dose rate was kept at 13 e/(Å^2·s).

Movie S7. Manipulating shape of AgCl nanocrystal by electron dose rate. The electron dose rate was kept at 13 e/(Å^2·s) at the beginning, then decreased to 1 e/(Å^2·s) as the brightness of the video shows.

Movie S8. Manipulating shape of AgCl nanocrystal by electron dose rate. The electron dose rate was kept at 13 e/(Å^2·s) at the beginning, then decreased to 1 e/(Å^2·s) as the brightness of the video shows.

Movie S9. Drifting and splitting of many AgCl nanocrystals. The drifting of nanocrystals was towards the observation window edge. The electron dose rate was kept at 13 e/(Å^2·s).

Movie S10. Drifting and splitting of many AgCl nanocrystals. Similar to Movie S9. The electron dose was kept around 19 e/(Å^2·s).

12. References

[1] N. D. Elkies, A. M. Odlyzko, J. A. Rush. *Invent. Math.* **1991,** *105*, 613-639.

[2] D. J. Audus, A. M. Hassan, E. J. Garboczi, J. F. Douglas. *Soft Mat.* **2015**.

[3] Z. Lou, B. Huang, X. Ma, X. Zhang, X. Qin, Z. Wang, Y. Dai, Y. Liu. *Chem.--Eur. J.* **2012,** *18*, 16090-16096.

[4] L. Rayleigh. *Philos. Mag. Ser. 5* **1882,** *14*, 184-186.

[5] O. Madelung, U. Rössler, M. Schulz, In *II-VI and I-VII Compounds; Semimagnetic Compounds*, Vol. 41B (Eds: O. Madelung, U. Rössler, M. Schulz), Springer, Heidelberg, Germany **1999**.

[6] J. B. Hasted, D. M. Ritson, C. H. Collie. *J. Chem. Phys.* **1948,** *16*, 1-21.

[7] Z. Aabdin, J. Lu, X. Zhu, U. Anand, N. D. Loh, H. Su, U. Mirsaidov. *Nano Lett.* **2014,** *14*, 6639-6643.

[8] D. T. Papageorgiou. *Phys. Fluids* **1995,** *7*, 1529-1544.

[9] H. Zheng, S. A. Claridge, A. M. Minor, A. P. Alivisatos, U. Dahmen. *Nano Lett.* **2009,** *9*, 2460-2465.

[10] L. Reimer, H. Kohl, *Transmission Electron Microscopy: Physics of Image Formation*. Springer, NY, USA **2008**.

[11] T. Tani, *Photographic Science: Advances in Nanoparticles, J-Aggregates, Dye Sensitization, and Organic Devices*. Oxford University Press, Oxford, UK **2011**.